Lithography Process Control Using Scatterometry Metrology and Semi-Physical Modeling

Kevin Lensing*[a], Jason Cain[a], Amogh Prabhu[a], Alok Vaid[a], Robert Chong[a], Richard Good[a], Bruno LaFontaine[b], and Oleg Kritsun[b]
[a]Advanced Micro Devices, 5204 E. Ben White Blvd., Austin, TX, 78741
[b]Advanced Micro Devices, One AMD Place, Sunnyvale, California 94088-3453

ABSTRACT

In this paper, results and analysis are presented from Advanced Micro Devices' (AMD) efforts at calculating lithography dose and focus parameters using scatterometry metrology and semi-physical CD models. The system takes advantage of the accurate and precise top and bottom CD data produced by scatterometry to differentiate dose and focus variation. To build the lithography process model, scatterometry data is generated for each field of a focus-exposure matrix (FEM) wafer, and the resulting top and bottom CD data is used to fit the parameters of series expansions relating CD to dose and focus. When new CD data is generated, the models can be inverted to solve for dose and focus independently. Our methodology employs a flexible modeling and inversion approach in an attempt to make the technique applicable to any production film stack and any line spacing regime. The quality of the inversion results are highly correlated to the degree of focus observability present in the system. Our results will show how a series of litho process with varied film stacks and line/space ratios respond to this technique, and we will report some best practices for a variety of use cases ranging from equipment characterization to focus monitoring on product.

Keywords: lithography modeling, scatterometry, focus control, statistical process control (SPC), advanced process control (APC), Bossung plots

1. INTRODUCTION

As semiconductor device technology migrates to the 45-nm node and beyond, process capability for critical lithography steps are becoming increasingly difficult to maintain. At previous technology nodes, the depth-of-focus (DOF) for critical patterning layers was large enough to assume that focus variation would not have a significant impact on output quality metrics. As this assumption becomes less realistic, new methodologies are needed to control focus. On the equipment side, traditional techniques for periodic calibration of machine focus are proving incapable of addressing subtle variations that occur on product at small geometries. On product, run-to-run APC control of critical dimensions (CD) using exposure dose alone relies on the underlying assumption that focus deviations will not significantly impact the approximately linear relationship between dose and CD. To address these emerging problems, AMD has developed a methodology to calculate critical dose and focus parameters using scatterometry metrology and semi-physical CD models. The system takes advantage of the sidewall profile metrology produced by scatterometry to provide the required focus sensitivity to detect subtle equipment variations before they negatively impact yield. The technique uses production film stacks and design-rule line spacing to ensure that the results are applicable to current products.

1.1 Existing Focus Control Techniques

A number of techniques are available for characterizing exposure-tool focus. Methods based on the use of special reticles producing non-telecentric imaging at the wafer plane convert an out-of-focus condition into an overlay error. Phase-shift focus monitoring (PSFM)[1,2], phase grating focus monitoring (PGFM)[3] and Z-SPIN[4] are some examples in this category. These methods require non-standard reticle and exposure conditions, making them applicable for characterizing and calibrating lithography equipment, but not for setting up or monitoring individual lithography processes.

Metrology, Inspection, and Process Control for Microlithography XXI, edited by Chas N. Archie
Proc. of SPIE Vol. 6518, 651804, (2007) · 0277-786X/07/$18 · doi: 10.1117/12.711548

The most common method for setting up process-specific dose and focus conditions is the systematic analysis of focus-exposure matrix (FEM) data. Historically this has consisted of plotting Bossung curves from a single CD-SEM metric and choosing the best focus value to achieve the target CD with the largest depth-of-focus (DOF)[5]. But this method does not present an opportunity for continuously monitoring focus at nominal production conditions. Recent publications have focused on creating focus and dose response models from FEM experiments, then applying those models to standard production conditions for continuous dose and focus monitoring. One method uses an optical imaging technique to measure line-end shortening (LES)[6,7,8,9] patterns. This method does show promising focus sensitivity, but it requires special test structures and does not provide the precise magnitude and direction of change information that would be required for making immediate corrections. Another method involves using scatterometry data to fit FEM models for two different points on the resist profile, thereby enabling independent solutions for dose and focus[10]. It is this general method that we will expound upon in this paper.

1.2 Scatterometry Metrology

The focus control solution detailed herein requires accurate, precise and reliable top and bottom CD data to adequately differentiate dose and focus variation. To that end, scatterometry metrology is being used rather than scanning electron microscopy (SEM). The top-down nature of CD-SEM renders it incapable of producing accurate sidewall information, especially at current geometries where critical resist lines are often densely nested and extremely vertical[11]. But while scatterometry solves the resist profile problem, it presents myriad challenges of its own. Scatterometry is a model-based technique that matches optical broadband spectra gathered from a diffraction grating on the surface of the wafer to a simulated response based on geometric shape and material property inputs. As a result, each new application requires a significant development effort to build a model, and model sensitivity to the parameters of interest is not guaranteed. The quality of the metrology result is generally a function of the composition of the film stack and the layout of the diffraction grating [12]. Film stack issues are becoming more problematic for lithography processes at 65-nm and beyond, as advanced anti-reflective coatings (ARC) become more efficient at eliminating the very reflectance that normal-incidence scatterometry relies upon for sensitivity to CD and resist profile variation. The layout of the grating poses a very specific challenge to this modeling application. CD sensitivity to focus changes generally increases as lines vary from nested to isolated, but scatterometry sensitivity to profile variation shows the opposite trend. This problem will be discussed in detail in Section 3 of this paper.

1.3 Use Modes

Potential use cases for this technique are quite varied. In this paper we will discuss how it can be used to characterize the focus uniformity performance of immersion scanners. In manufacturing, we can use this method for periodic calibration of machine focus. By measuring in a variety of locations across the reticle field in both horizontal and vertical orientations, calibration results can be expanded to include monitoring of focus uniformity, reticle tilt, astigmatism, chuck flatness, wafer edge effects, and other critical lithography parameters. For characterization and calibration of equipment, it is possible to engineer the test vehicle to guarantee optimal performance. Since there are no process-related restrictions, simple experiments can reveal the best line spacing regime, focus and exposure settings, and film stack to produce accurate model-predicted dose and focus values. One can choose to operate at process settings that are intentionally skewed from the flat portion of the process window, thereby insuring that small changes in dose and focus are reflected as changes in top and bottom CD values.

The real novelty of this method, however, is the potential for in-line product monitoring with no additional measurement or real-estate overhead. For cases where scatterometry metrology is already being utilized in production for lithography process control, it would be ideal to use that data to differentiate dose and focus errors in near real-time. As a statistical process control (SPC) method, one could simply monitor focus variation and halt the equipment in the case of an excursion. As an advanced process control (APC) method, dose and focus could both be corrected on a run-by-run basis, enabling seamless transition to technology nodes with severe depth-of-focus (DOF) problems.

The challenge associated with using this method for product monitoring is that the flexibility for test vehicle optimization is largely absent. The film stack is obviously not open to change, and the focus and exposure settings have already been optimized to maximize the process window. While this is great for production stability, it tends to diminish the effectiveness of our monitoring technique by placing the process in a region where the CD's do not change

significantly with small changes in focus. It is also likely that the critical line spacing has already been chosen by production based on process limiting design rules. For many layers, product is dispositioned based on densely nested features, which again diminishes focus sensitivity. One approach to this problem is to measure a dense disposition structure and an isolated focus structure, but this solution doubles both the measurement time and the test structure real estate requirement. The challenge we will seek to address in this paper is how to create a modeling approach that can be optimized for any lithography system, enabling dose and focus monitoring on product to support SPC and APC applications without adding additional infrastructure burden.

2. METHODOLOGY

2.1 Focus-Exposure Model Structure

The choice of a proper model for the CD response to exposure dose (E) and focus (F) is critical in achieving meaningful and high-quality model fits. Most early efforts to fit such data relied on models with polynomial terms in focus and exposure. In general these models take the form

$$CD = \sum_{i=0}^{M} \sum_{j=0}^{N} a_{ij} E^i F^j \tag{1}$$

where $M = 3$ and $N = 4$ are typical values. Several terms in these models are often fixed at zero, bringing the total number of fitting parameters to 12-14.

Determining the appropriate number of model terms to use in order to obtain a good fit to the real variation in the data without over-fitting to noise is difficult. Mack and Byers proposed such a model[13] based on a Taylor expansion of the first few terms of the Fourier series representation of the one-dimensional aerial image. This model assumes a thin, infinite contrast resist is removed when the exposure dose exceeds a threshold value. This approximation leads to a different form for the exposure dose terms and the full model may be written as

$$CD = \sum_{i=0}^{M} \sum_{j=0}^{N} a_{ij} \left(1 - \frac{E_s}{E}\right)^i F^j \tag{2}$$

where E_s is a constant representing the exposure dose required to achieve the target CD. Here, $M = 3$ and $N = 4$ are practical upper bounds on the number of model terms although the exact form of the model is process-dependent. This model form is used throughout the remainder of this work to develop models unique to individual lithographic processes.

It will prove useful to invert the model in order to estimate exposure dose and focus based on measured CD values. However, it is not possible to determine a unique value for dose and focus based on a single CD measurement. Ausschnitt and Cheng proposed[10] to take advantage of the physical focus offset between the top and bottom of a line that results in different behavior of top and bottom CD under dose and focus variation. This leads to a system of two equations in two unknowns that may be solved for unique dose and focus values. Starting from Eq. (2) and combining similar terms, this system can be expressed as

$$CD_{top} = \sum_{i=0}^{M} \sum_{j=0}^{N} a_{ij} \frac{F^j}{E^i} \quad \text{and} \quad CD_{bottom} = \sum_{i=0}^{M} \sum_{j=0}^{N} b_{ij} \frac{F^j}{E^i} \ . \tag{3) and (4}$$

Note that in this formulation the coefficients for a given equation are linear combinations of the coefficients that would be obtained under the formulation showed in Eq. (2).

2.2 Model Fitting

The values of m and n that are used in Equations (3) and (4) vary the predicted CD values to a large extent. The optimum values of m and n for a given dataset are best determined by regressing the parameters for each (m,n) model and then looking at the various statistics like the R^2 value and mean squared error (MSE) of the fit. Again we refer to Ausschnitt and Cheng, who propose using a truncated form of the (2,1) [11]

$$CD = a_{00} + a_{10}\left(1 - \frac{E_s}{E}\right) + a_{20}\left(1 - \frac{E_s}{E}\right)^2 + a_{02}\left(F - F_0 - S\right)^2 \quad . \tag{5}$$

In this approach, (E_s) and (F_o) are the dose and focus combination that will produce the desired bottom CD with the maximum depth of focus, and (S) represents the intrinsic focus offset between the top and bottom of the resist feature. These parameters are absorbed into the model parameters a_{nm} in the model proposed in Equations (3) and (4). Equation (5) also assumes that the focus asymmetry terms a_{n1} are negligible, and the dose-defocus decoupling term a_{12} is discarded with the caveat that the sample pattern must be isolated or semi-isolated.

The advantage of (5) is that it is quadratic in nature, which can be solved readily in an analytic form to give the effective dose and focus values. The disadvantage is that the equation is only applicable to patterns that exhibit parabolic response to focus. In our attempt to formulate a model structure that would accommodate a variety of lithography systems, including those that are constrained by manufacturing limitations, we found that our experimental FEM scatterometry results required higher model orders to adequately fit the sample data. In the majority of cases, the (4,1) model was found to be most satisfactory since it included the complexity of the dependence on focus while at the same time avoiding excessive parameters that fit to process noise. But in general, the optimal model order is inversely proportional to the amount of noise in the sample FEM data, and some degree of process knowledge must be applied to ensure that the model structure is reflective of a physically achievable response surface.

Let us consider an exemplary production lithography layer that we will refer to as Process A. In Figure 1 we see that Process A exhibits a bottom CD response surface that can not be adequately modeled by the 6-term (2,1) version of the series expansion. This is not surprising since the scatterometry grating for process A has a 1:2 line-to-space ratio, resulting in an isofocal region where the bottom CD does not change with focus and therefore can not be fit to a parabolic model. The 10-term (4,1) model captures that region of the response surface much better, and this fact is reflected in a significant improvement in the fit statistic. Conversely, as we move to the 20-term (4,3) model, the fit does not improve significantly, and the Bossung curves start to take on a counter-intuitive level of complexity.

Table 1 shows how this general method can be applied to data sets ranging from noisy (Process B) to noiseless (simulated Process C) metrology. The fit statistics will generally show a significant improvement any time that the data set supports a higher order model. As the models start fitting to noise, the fit statistics will show minimal improvement with higher model order. Since Process C is actually the CD output from a noiseless lithography simulation, it is not surprising to see that the MSE approaches zero as the number of terms increases, but in our experience, no real process has ever supported the (4,3) structure.

Table 1. Model fit statistics for three process examples ranging from high to low noise levels, modeled using 6, 10, and 20 parameter series expansions. Green shading indicates the selected model order.

Process B (noisy)		6 parameter (2,1)	10 parameter (4,1)	20 parameter (4,3)
Bottom	R^2	0.9717	0.9725	0.9793
	MSE	2.21	2.19	1.90
Top	R^2	0.8818	0.9064	0.9226
	MSE	2.41	2.14	1.95
Process A (moderate)				
Bottom	R^2	0.8789	0.9637	0.9756
	MSE	6.02	3.29	2.70
Top	R^2	0.9778	0.9879	0.9917
	MSE	3.23	2.38	1.98
Process C (noiseless)				
Bottom	R^2	0.9951	0.9955	0.9997
	MSE	0.87	0.82	0.22
Top	R^2	0.9635	0.9864	0.9978
	MSE	3.33	2.03	0.81

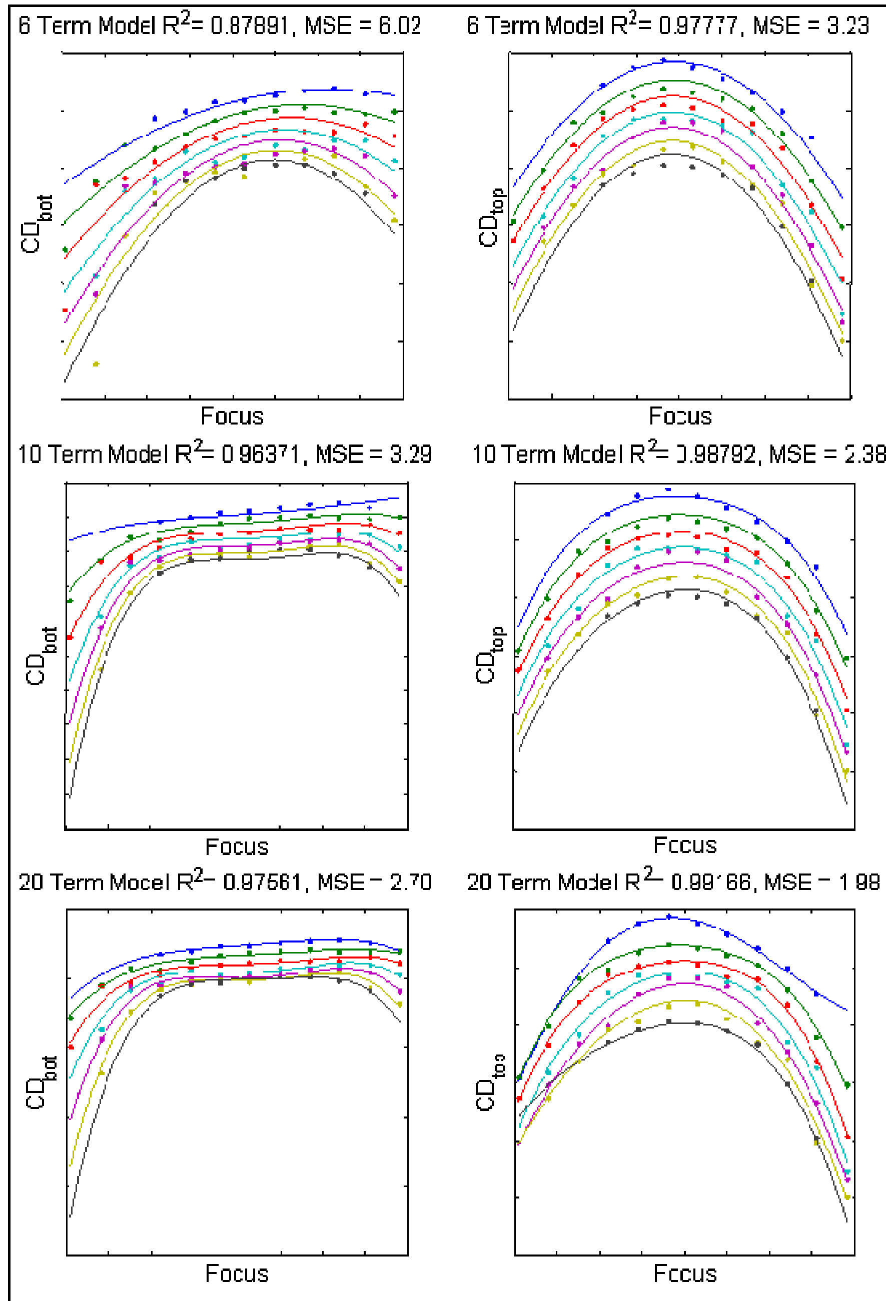

Figure 1. Bossung plots of Process A using 6, 10, and 20 parameter models. Raw data is represented by dots and model fits are represented by solid lines. In this case, the 10-parameter model was chosen as optimum.

2.3 Model Inversion

To this point we have discussed using FEM data to map commanded focus and dose to line-width measurements. Once this model has been created for CDs at the top and bottom of the resist profile, the model can be inverted to estimate the focus and exposure-dose from these CD measurements. Essentially, we are tasked with solving two equations for two unknowns. As an example, let us consider the 10-parameter polynomial expansion for our two relevant CDs.

$$CD = a_{00} + a_{01}F + a_{02}F^2 + a_{03}F^3 + a_{04}F^4 + a_{10}\frac{1}{E} + a_{11}\frac{F}{E} + a_{12}\frac{F^2}{E} + a_{13}\frac{F^3}{E} + a_{14}\frac{F^4}{E} \quad (6)$$

Here a well-known algebraic technique can be used along with a polynomial root finder to solve for the focus and dose as a function of our two CDs. The solution is provided in the appendix. As noted in Section 2.2, it has been found that this 10 parameter model is appropriate for most lithography systems with moderate noise levels. If a higher order model is required then the analytical solutions become prohibitively complicated. By adding a quadratic term in exposure (i.e., m=2) then the analytic solution includes 32 complex roots. A numerical solver should be used for these higher order models.

The inversion of the 10-parameter model returns eight complex solutions. Since imaginary dose and focus values are not physically realizable, we need only consider the real solutions. And, if second-order (or higher) terms are used in the model then we will always have multiple solutions. It is therefore necessary to look at two scenarios: when the inversion provides multiple real solutions and when the inversion provides no real solutions. To illustrate these two scenarios, let us consider an arbitrary Process D with scatterometry FEM results that have been modeled using the 10-parameter form from equation (6) for top and bottom CD.

If a bottom CD of "X" and a top CD of "Y" is measured, the model inversion returns the eight roots shown in Table 2a. Here we see that six of the eight roots are complex (and therefore physically unattainable) and two of the roots are real. This means that, according to the model, there exists two dose and focus combinations that will produce values of X and Y for the bottom and top CDs, respectively. In this case the solution closest to the commanded dose and focus should be considered the correct value.

If the top CD measurement drops to "Y – 4" then the model inversion returns the roots shown in Table 2b. In this case all of the solutions are complex and, according to the model, there exists no focus and dose values that will return exactly X and Y - 4. In this case, a numerical technique can be used to find the dose and focus values that return CDs as close as possible to the measured CDs.

Table 2. Analytical solutions to an exemplary 10-parameter (4,1) model at two different top CD values.

a) Analytical solutions for CD = [X Y]		b) Analytical solutions for CD = [X Y-4]	
Focus (Inv)	Dose (Inv)	Focus (Inv)	Dose (Inv)
-0.2192 + 0.0766i	22.9998 - 0.9077i	-0.2223 + 0.0802i	23.0603 - 0.8691i
-0.2192 - 0.0766i	22.9998 + 0.9077i	-0.2223 - 0.0802i	23.0603 + 0.8691i
-0.1519 + 0.0509i	44.4004 +28.5837i	-0.1526 + 0.0508i	39.4518 +44.2853i
-0.1519 - 0.0509i	44.4004 -28.5837i	-0.1526 - 0.0508i	39.4518 -44.2853i
-0.065	25.4811	-0.0079 + 0.0395i	22.7177 - 0.2217i
-0.0155 + 0.0373i	22.5028 - 0.7271i	-0.0079 - 0.0395i	22.7177 + 0.2217i
-0.0155 - 0.0373i	22.5028 + 0.7271i	-0.0424 + 0.0169i	25.1633 - 0.7162i
-0.0123	23.7868	-0.0424 - 0.0169i	25.1633 + 0.7162i

The numerical technique we chose seeks to minimize the sum of the squared errors according to the following expression, where *Error* is simply the difference between the actual and the model-predicted CD value:

$$\min_{BotCD,TopCD} J = Error_{BotCD}^2 + Error_{TopCD}^2 \quad (7)$$

Figure 2 shows the numerical solutions for the CD values in Table 1 in terms of a contour plot. The blue lines express the minimum values of the objective function while the red lines express a higher value. The real parts of the analytical roots are shown as black stars. In Figure 2a, we see that the numerical solver finds minima identical to the two real roots of the analytical solution. If we initialize the optimization with the commanded dose and focus values and use a steepest-descent optimization methodology, it follows that the solver will choose the minima closest to the initial conditions. This outcome matches our recommended procedure for choosing between real analytical roots. In Figure 2b, we see that the numerical solver finds a single minimum that is close to, but not exactly the same as, the real part of one of the complex analytical roots. As mentioned above, for this case we would clearly prefer the numerical solution. Given that the numerical solver is able to match the performance of the analytical method for the case where there are real roots and exceed it where all the roots are complex; we choose to employ the numerical method exclusively for all of our model inversions.

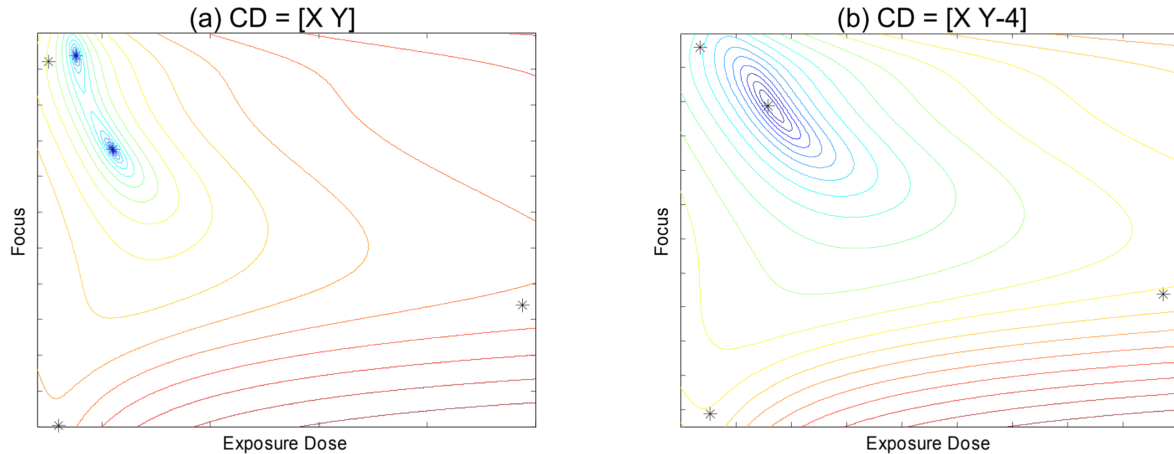

Figure 2: Figures (a) and (b) are contour Plots of the Numerical Solution for the two CD examples in Table 2. Stars show real part of analytical solutions.

3. FOCUS OBSERVABILITY

While choosing the correct model order and inversion technique are critical to achieving good results, in many ways the lithography process itself dictates the limits of success. In control theory, observability is a measure for how well internal states of a system can be inferred by knowledge of its external outputs. In our case, we must be able to observe small changes in dose and focus as independent changes in the response of one or both of the modeled CD parameters. This is generally a simple requirement for dose, but a complex requirement for focus. Even if the model fits are near unity, the solver will find a wide range of nearly equivalent inversion results if the Bossung plots are flat in their response to focus. As mentioned in Section 1, the test vehicle can be engineered for good focus observability if the objective is to calibrate or characterize a lithography scanner. But if the objective is to work within the bounds of existing infrastructure for production layers, it is likely (and favorable for manufacturing) that one or both of the CD parameters will lack focus response in some portion of the process window. As we move to more advanced technology nodes, this problem actually diminishes, since the DOF scales down with feature size. But in the interim, as we seek to test our method on more forgiving processes, it is critical to understand the amount of focus observability in the system in order to correctly interpret inversion results.

One way to check for focus observability is simply to perform the inversion routine on the experimental FEM data set and look at the correlation between commanded and model-predicted parameter values. Poor focus observability will be clearly indicated in the commanded versus estimated focus correlation as a large spread about the mean in the estimated values for some portion of the FEM. Figure 3 shows the modeling and inversion self-check results from Process E. Here we see that the model fits are excellent, but the process response to focus is poor, especially in the center of the experimental range. This is clearly reflected in the focus inversion plot, where the spread in predicted values in the center of the FEM is quite large. Where the Bossung curves show more shape at the focus extremes, the range of predicted values is much smaller. Conversely, Figure 4 shows the modeling and inversion self-check results for Process F, which exhibits much better focus observability. This can be seen in the shape of the Bossung plots and in the quality of the focus inversion correlation plot. Note that Processes E and F were both fit with 10-parameter (4,1) models, and that the range of experimental focus values is nearly equivalent.

Processes E and F are also indicative of how the challenge of engineering this application differs based on use mode. Process E is a 65-nm production lithography layer, where our objective is to use the scatterometry infrastructure that is already implemented in manufacturing to enable dose and focus extraction. While it is true that Process E shows an especially large DOF, it is nonetheless illustrative of the general point that current lithography processes are likely to have an isofocal region in the center of the process window where the resolution of the focus inversion routine will be low. It is our desire to develop a generalized dampening metric based on the degree of observability as a function of focus that will ensure that any SPC or APC system will not react to inversion noise in such cases.

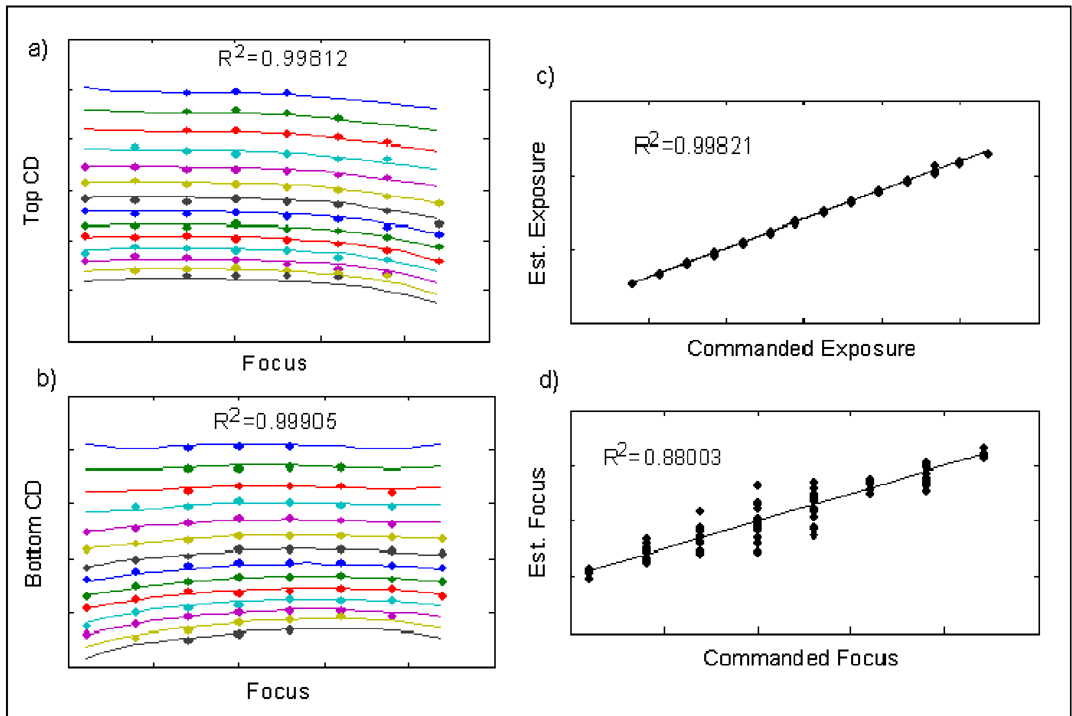

Figure 3. Bossung plots and inversion results from Process E. In figure (d) we see that the lack of focus response in the center of the FEM range translates into a large spread in estimated focus values. Note that the R^2 statistics for all the inversion self check plots, including figures (c) and (d), have a slope of unity and intercept of zero.

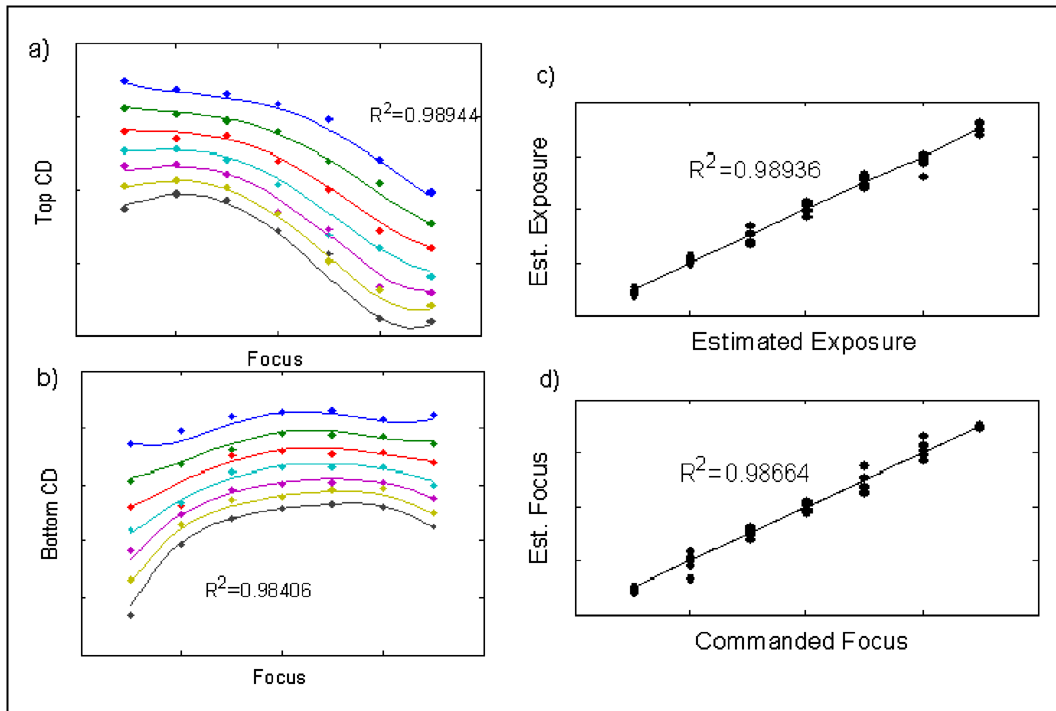

Figure 4. Bossung plots and inversion results from Process F. In figure (d) we see that good focus observability throughout the FEM range results in a much better correlation between commanded and estimated focus values.

Process F represents the optimized form of the FEM model used to characterize the ASML 1700i hyper-NA immersion scanner in Section 4. In this case, it was possible to select the exposure conditions and the line spacing regime that would produce enough focus observability to calculate focus deviations on the nanometer scale. As mentioned in Section 1, it is generally true that focus sensitivity increases as patterns become more isolated, but scatterometry sensitivity to the line profile shows the opposite relationship. Our approach to solving this problem is to simulate scatterometry performance through pitch and select the maximum degree of isolation that the scatterometry model will support. Figure 5 shows the result of this analysis for Process F.

The film stack used for Process F consists of patterned resist on top of BARC with a silicon substrate. The floating model parameters for the scatterometry model include the CD at the top of the resist line, the CD at the bottom of the resist line, the thickness of the patterned resist and the thickness of the BARC. Figure 5a shows the sensitivity of each parameter in terms of a 3-sigma precision value, such that a lower value represents a more sensitive parameter and therefore a "better" result. Here we see that no individual parameter fails the sensitivity bounds until the space is seven times larger than the line. But it is not enough that each parameter is individually sensitive. Additionally, it is important to avoid a condition where one floating parameter is an order of magnitude more sensitive than another, and at a 1:4 ratio the BARC becomes ten times more sensitive than the top CD. Figure 5b shows the degree of correlation between any two floating parameters in our scatterometry model. Parameters are correlated when similarities in material properties make it impossible for the scatterometry model to assign a change in the raw spectra to a single parameter. Here we see that the top CD and the resist height become correlated at greater than our 80% limit at 1:4. With multiple metrics showing scatterometry marginalities at a 1:4 line-to-space ratio, we chose to use a 1:3 structure for our application.

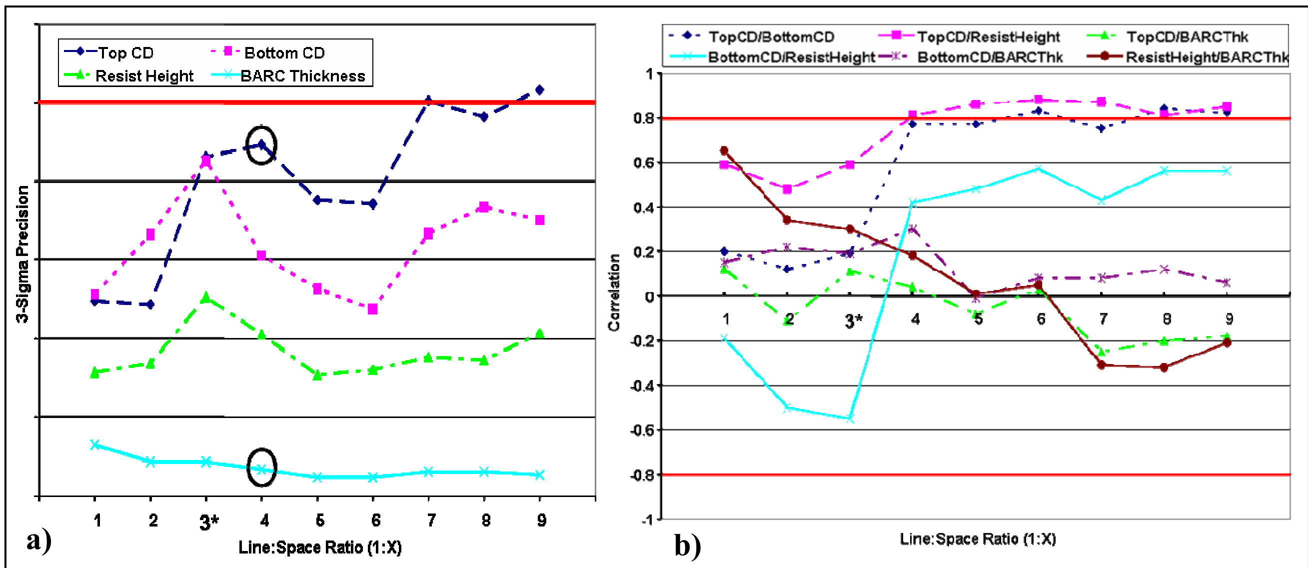

Figure 5. Scatterometry simulation results for a single line size through pitch for Process F. Figure a) shows the sensitivity of each floating parameter as a function of spacing. The circles indicate where the top CD and the BARC thickness reach a 10x disparity. Figure b) shows parameter correlation as a function of spacing, with the correlation between top CD and resist height failing at 1:4.

4. APPLIED RESULTS

4.1 Reticle Tilt

One lithography equipment metric that must be regularly calibrated is the scanned image tilt. Tilt refers to the angle that the best-focus image plane forms relative to the wafer surface. If the scanned image is tilted top-to-bottom or left-to-right, the problem will be manifested as variation in effective focus values across the image field. It is a common practice to regularly measure features in the corners of the field to monitor for tilt issues. Historically it has been difficult to translate those corner CD measurements into actual focus values for tilt calibration, but by using FEM models to invert top and bottom CD measurements, we can measure reticle tilt in the X and Y direction with relative ease.

To test our ability to accurately measure the image tilt, we exposed one wafer with no tilt and another wafer with a programmed 6 microradians (μrad) of tilt along the length of the scanner slit. The 10-parameter (4,1) model for Process

A (see Figure 1b) was used to invert top and bottom CD values for each corner of the reticle field and every field on the wafer. The average effective focus value from each corner location was then used to calculate the degree of tilt along the length of the scanner slit. Table 3 shows that our application was able to accurately detect the presence of reticle tilt. Note that the left-to-right focus bias is converted to radians of tilt by taking the arctangent of the quotient of the focus offset and the distance between the two y-axis measurements.

Table 3. Results of tilt calculation experiments using the 10-parameter (4,1) model for Process A.

	Average Focus Value	
Location	**6 μrad Tilt**	**No Tilt**
Lower Left (μm)	-0.092	0.000
Lower Right (μm)	0.030	0.013
Upper Left (μm)	-0.080	-0.008
Upper Right (μm)	0.020	-0.002
Left-Right Bias (μm)	0.111	0.010
Calculated Ry Tilt (μrad)	**6.11**	**0.52**

4.2 Dose and Focus Uniformity

When attempting to characterize the performance baseline of a lithography tool, it is desirable to measure any systematic non-uniformity in dose and focus across the wafer surface. The two dominant modes of systematic non-uniformity are across the image field and across the wafer. Uniformity maps can be created by measuring multiple points in the field and all fields on the wafer, then inverting the data and plotting the results on a contour map. These maps can be used to identify systematic chuck flatness issues, edge effects, reticle shape, and a variety of other potential problems.

As mentioned in Section 3, Process F represents a system optimized for characterization of an ASML 1700i hyper-NA scanner. To check across-wafer and intra-field performance of the scanner, wafers were printed at optimal focus and dose settings. Scatterometry was used to measure ~16 points/field for the complete wafer. Both horizontal and vertical gratings were measured. Bottom and top CD data was inverted to produce dose and focus values for each measurement location. Figure (6a) and (6b) shows this average across-wafer focus and dose variations determined from scatterometry models. It can be difficult to interpret inversion uniformity results because the application interprets any and all variation in top and bottom CD as an indication of dose or focus non-uniformity. In fact, we know that CD variance comes from a variety of sources not related to dose or focus: reticle write errors, FEM model mismatch, process and metrology noise, etc. In order to calculate real dose and focus variation, it is desirable to measure and remove systematic sources of CD variation that are not related to dose and focus errors. Most notably, reticle effects should be de-convoluted in order to achieve an accurate analysis of scanner performance. This would ideally be accomplished by directly measuring the reticle and normalizing the CD data for the reticle signature prior to modeling and inversion. In the absence of any reticle CD measurements, it is reasonable to assume that the average across-field variance in each CD parameter is due primarily to the reticle. Figures (6a) and (6b) have been corrected for reticle effects in this manner, and we see that most of the residual variance is related to wafer edge effects.

Figure (6c) and (6d) show average intra-field focus and astigmatism variations of the same data. Astigmatism values are approximated by analyzing the distribution of focus offsets between vertical and horizontal measurements. In this case, the data has not been corrected in order to highlight the systematic variation that is revealed by this technique. The field signatures for focus and astigmatism both indicate the need for reticle shape and tilt corrections, and these results have been shown to correlate well with results from an alternative focus monitoring technique[14].

5. CONCLUSIONS

In this paper we have presented a modified version of the methodology developed by Ausschnitt and Cheng for using scatterometry data and semi-physical modeling to extract the effective dose and focus at the wafer surface. By utilizing a flexible modeling structure and the appropriate numerical solver and objective function, we are able to accommodate a wide variety of litho systems with varying degrees of noise and focus observability. Our goal in this effort is to enable use modes ranging from equipment calibration and characterization to production monitoring for active process control. Results reported from a variety of processes indicate that, while it is possible to achieve excellent model fits for most

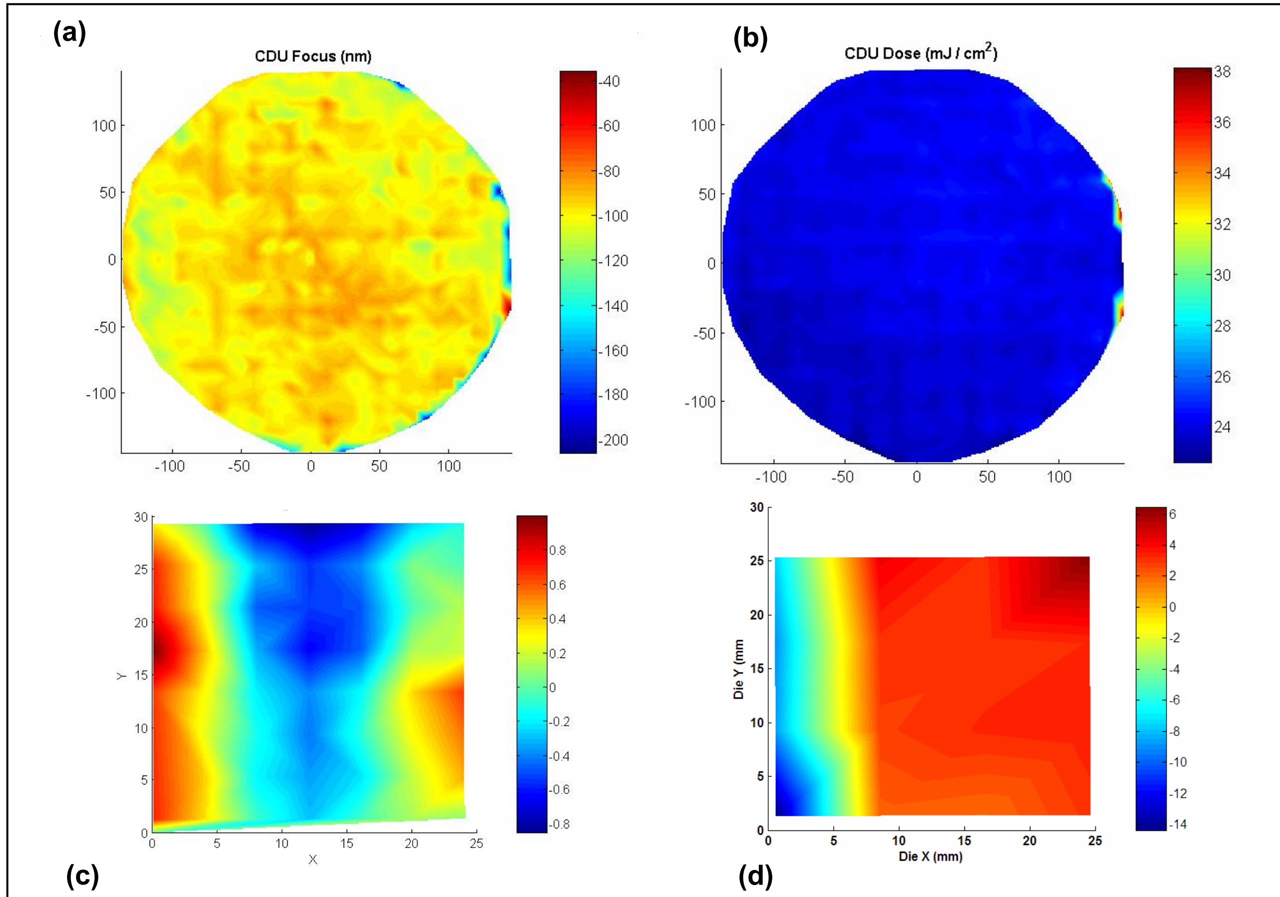

Figure 6. Figures (a) and (b) show across-wafer focus and dose variations determined from scatterometry models. Figures (c) and (d) show average intra-field variation of focus and astigmatism, respectively, from the same data.

processes by allowing higher order terms, there is likely to be an isofocal region for most manufacturing processes that will result in poor inversion results independent of model fidelity. The results of two practical applications show that, when focus can be observed, accurate and useful metrics can be calculated and used for equipment and process engineering.

Future work will largely be related to refining the application for use as an in-line product monitor. It is important that the application not induce erroneous responses when a process is operating in a regime of poor focus sensitivity. In practical application, that means ensuring that there is a statistically significant signal before flagging a process for a focus-related SPC failure. As the depth-of-focus shrinks for critical lithography processes at future technology nodes, the ultimate application of this technique will be for simultaneous APC run-to-run control of dose and focus. By relying on an automated system to correct for focus deviations, lithography engineers can be freed from the increasingly difficult task of developing processes with a depth-of-focus at the target CD that is large enough to withstand the expected process and equipment variation. In fact, the isofocal region is actually the enemy of process control, since it diminishes our ability to observe focus changes. The challenge of developing a multi-input, multi-output (MIMO) APC controller based on this application is significant but certainly achievable. The greater challenge will be convincing lithography engineers to shift their processes away from best focus to ensure a robust model for APC control.

APPENDIX

In this section the analytical solution to the inversion of the polynomial models shown in (3) and (4) is provided. First, the focus value is determined by solving for the roots of the 8-order polynomial

$$f = z_0 + z_1 x + z_2 x^2 + z_3 x^3 + z_4 x^4 + z_5 x^5 + z_6 x^6 + z_7 x^7 + z_8 x^8 \quad (8)$$

where

$$z_0 = (a_{00} - CD_1)b_{01} - a_{01}(b_{00} - CD_2)$$

$$z_1 = -a_{01}b_{10} + b_{11}(a_{00} - CD_1) - a_{11}(b_{00} - CD_2) + b_{01}a_{10}$$

$$z_2 = b_{11}a_{10} + (a_{00} - CD_1)b_{21} - a_{11}b_{10} - a_{01}b_{20} - a_{21}(b_{00} - CD_2) + a_{20}b_{01}$$

$$z_3 = -a_{31}(b_{00} - CD_2) + b_{01}a_{30} - a_{21}b_{10} - a_{01}b_{30} + b_{31}(a_{00} - CD_1) + b_{11}a_{20} + b_{21}a_{10} - a_{11}b_{20}$$

$$z_4 = b_{31}a_{10} + (a_{00} - CD_1)b_{41} + a_{20}b_{21} - a_{41}(b_{00} - CD_2) - a_{01}b_{40} - a_{11}b_{30} + b_{11}a_{30} - a_{21}b_{20} + a_{40}b_{01} - a_{31}b_{10}$$

$$z_5 = b_{41}a_{10} - a_{41}b_{10} + b_{31}a_{20} - a_{11}b_{40} + b_{11}a_{40} + b_{21}a_{30} - a_{31}b_{20} - a_{21}b_{30}$$

$$z_6 = -a_{41}b_{20} + b_{31}a_{30} + a_{40}b_{21} - a_{31}b_{30} + a_{20}b_{41} - a_{21}b_{40}$$

$$z_7 = b_{31}a_{40} - a_{31}b_{40} + b_{41}a_{30} - a_{41}b_{30}$$

$$z_8 = a_{40}b_{41} - a_{41}b_{40}.$$

Next, the eight roots of (3) are substituted back into (1) or (2) to solve for the corresponding dose values,

$$E = \frac{b_{01} + b_{11}f + b_{21}f^2 + b_{31}f^3 + b_{41}f^4}{b_{00} + b_{10}f + b_{20}f^2 + b_{30}f^3 + b_{40}f^4}. \quad (9)$$

REFERENCES

1. T. A. Brunner et al., " Optical focus phase shift test pattern, monitoring system and process," US patent 5,300,786 (1994)
2. K. Izhuha et al., "Novel in situ focus monitor technology in attenuated PSM," *Proc., SPIE* 5040, 590-595 (2003).
3. B. La Fontaine et al., "Phase grating focus monitoring using overlay technique," US patent 6,710,853 (2004).
4. Y. Shiode et al. "A novel focus monitoring method using double side chrome mask," *Proc., SPIE* 5754, 303-314 (2005).
5. J. W. Bossung, "Projection Printing Characterization," *Developments in Semiconductor Microlithography II, Proc., SPIE* 100, 80-84 (1977).
6. C. P. Ausschnitt, "Distinguishing dose from defocus for in-line lithography control," *Proc., SPIE* 3677, 140-147 (1999).
7. B. Eichelberger, B. Dinu, H. Pedut, "Simultaneous Dose and Focus Monitoring on Product Wafers," in *Metrology, Inspection, and Process Control for Microlithography XVII,* Daniel J. Herr, ed., Proc. SPIE **5038**, pp. 247-254, 2003.
8. B. Dinu et al. "Effect of inline dose and focus monitoring and control on post etch CD," *Proc., SPIE* 5375, 1004-1009 (2004).
9. L. Armellin et al. " Simultaneous dose-focus monitoring on production wafers," *Proc., SPIE* 5752, 815-826 (2005).
10. C. P. Ausschnitt et al. "Modeling for profile-based process-window metrology," *Proc., SPIE* 5378, 38-47 (2004).
11. Kevin R. Lensing et al, "A Comprehensive Comparison of Spectral Scatterometry Hardware," in *Metrology, Inspection, and Process Control for Microlithography XIX*, Richard M. Silver, ed., Proc. SPIE **5752**, 2005.
12. K. Lensing and B. Stirton, "Integrated Metrology and Wafer-Level Control," Semiconductor International, June 2006, pp 44-54.
13. Chris A. Mack and Jeffrey D. Byers, "Improved model for focus-exposure data analysis," in *Metrology, Inspection, and Process Control for Microlithography XVII*, Daniel J. Herr, ed., Proc. SPIE **5038**, pp. 396-405, 2003.
14. C. Saravanan et al., "Characterization of hyper-NA lithography focus control using scatterometry ," *Proc., SPIE* 6518 (2007).